http://dx.doi.org/10.5012/bkcs.2013.34.9.2795

Critical Enhancement of Photothermal Effect by Integrated Nanocomposites of Gold Nanorods and Iron Oxide on Graphene Oxide

Kum-Hee Yun, Sun-Hwa Seo, Bo-Mi Kim, Ara Joe, Hyo-Won Han, Jong-Young Kim,† and Eue-Soon Jang*

Department of Applied Chemistry, Kumoh National Institute of Technology, Gyeongbuk 730-701, Korea
**E-mail: euesoon@kumoh.ac.kr*
†Korea Institute of Ceramic Engineering & Technology
Received July 15, 2013, Accepted July 23, 2013

Irradiation of gold nanorods (GNRs) with laser light corresponding to the longitudinal surface plasmon oscillation results in rapid conversion of electromagnetic energy into heat, a phenomenon commonly known as the photothermal effect of GNRs. Herein, we propose a facile strategy for increasing the photothermal conversion efficiency of GNRs by integration to form graphene oxide (GO) nanocomposites. Moreover, conjugation of iron oxide (IO) with the GO-GNR nanohybrid allowed magnetic enrichment at a specific target site and the separated GO-IO-GNR assembly was rapidly heated by laser irradiation. The present GO-IO-GNR nanocomposites hold great promise for application in various biomedical fields, including surface enhanced Raman spectroscopy imaging, photoacoustic tomography imaging, magnetic resonance imaging, and photothermal cancer therapy.

Key Words : Photothermal effect, Longitudinal plasmon resonance, Gold nanorods, Iron oxide, Graphene oxide

Introduction

The recent rapid evolution of nanoscience and nanotechnology has propelled the development of various multifunctional solid nanoparticles with unique chemical and physical properties for biomedical applications as multimodal molecular imaging probes and therapeutic agents.[1-5] In many cases, however, the chemical toxicity of the metal ions, dissolved by the metabolic process, restricts the use of these species (*e.g.*, CdSe quantum dots) to clinical applications.[6,7] Thus, biocompatible materials such as gold, iron oxide, and silica nanoparticles are becoming choice of materials for biomedical applications.[1,2,8] Among them, gold nanorods (GNRs) grown anisotropically along the [001] direction have been extensively studied during the past decade because of their biocompatibility and excellent plasmonic responses.[9,10] In particular, longitudinal surface plasmon resonance (LSPR) of free electrons along the elongated axis of the GNR can be quickly converted to thermal energy through the lattice collisions, a feature that has recently been recognized to be highly promising for cancer therapy.[9] However, based on the penetration-depth limit of the laser source, the irradiation may be attenuated by adsorption and scattering processes in the tissue.[11] Thus, GNR-based photothermal studies have focused primarily on near-tissue diseases such as melanoma and breast cancer.[9,12,13] In this regard, enhancement of the photothermal conversion efficiency of GNR is mandatory for further progress of photothermal therapy. Nevertheless, relatively little research has been conducted in this direction, in contrast to the voluminous existing database on photothermal cancer therapy based on GNR.

The ultimate goal of the present study is to investigate the photothermal effect of a GNR assembly integrated into a graphene oxide (GO) nanosheet, which is an ideal substrate material for meeting our objective because of its high thermal conductivity (~5,000 $Wm^{-1}K^{-1}$) and high optical transmittance (~97.7%).[14,15] Furthermore, covalent conjugation of the GO-GNR nanohybrid structures with silica-coated iron oxide (Fe_3O_4@SiO_2) allows recycling of the GO-IO-GNR composites. As anticipated, magnetic separation of the GO-IO-GNR assembly brings about a local photothermal effect in the target site, which is demonstrated herein. To the best of our knowledge, the present study provides groundbreaking empirical evidence of the enhanced photothermal efficiency in GNR-integrated nanostructures.

Experimental

Graphene Oxide Nanosheet Colloid. The GO nanosheets were synthesized from graphite flakes using a modified Hummers method, as previously described.[16] Briefly, 0.5 g of graphite flakes (Duksan, cat # 798) was oxidized in a 20 mL flask by adding a concentrated H_2SO_4 and H_3PO_4 (9:1) mixture. Then, 2.5 g of $KMnO_4$ (Sigma-Aldrich) was slowly added while stirring at 35 °C for 2 h. The resulting solution was cooled to 3-4 °C in an ice bath, and 300 mL of distilled water (DI) containing 1 mL of 30% H_2O_2 was added to eliminate the excess $KMnO_4$ while maintaining the temperature at 7 °C and stirring at 300 rpm. The resulting product was filtered using a cellulose acetate membrane with a pore size of 450 nm; the remaining solids were further purified and washed by rinsing and centrifugation with 10% HCl for several repetitions. Finally, the product was vacuum dried overnight.

Synthesis of Fe_3O_4@SiO_2 Nanoparticles. Oleic-acid-

coated Fe_3O_4 nanoparticles (13 ± 2.5 nm in diameter) were provided by Ocean Nanotech LLC; silica-coated Fe_3O_4 nanoparticles were prepared *via* a reverse microemulsion process according to a previous report.[17] In a typical procedure, 300 μL of bare Fe_3O_4 nanoparticles was suspended in 29.2 mL of cyclohexane (Sigma-Aldrich) with mild stirring, and 560 μL of Triton-X100 (Sigma-Aldrich) and 22.4 μL of NH_4OH (29.3 wt %, Sigma-Aldrich) were then added to the solution. The clear dark brown solution became turbid upon addition of NH_4OH. A stable reverse microemulsion was generated by adding 40 mM of 1-octanol such that the resulting solution became optically transparent. Addition of 165 mM tetraethylorthosilicate (TEOS, Sigma Aldrich) to the solution resulted in the immediate hydrolysis of the TEOS. Growth of the silica layer was allowed to continue with vigorous stirring at 600 rpm for 72 h at room temperature. The reaction was terminated by addition of acetone before removal of the excess organic components through centrifugation at 15,000 rpm for 30 min.

Gold Nanorod Solution. The GNRs were prepared by following the seed-mediated procedure developed by Murphy and coworkers.[18] The seed solution was synthesized by mixing 5 mL of 0.2 M hexadecylcetyltrimethylammonium bromide (CTAB) aqueous solution with 5 mL of 0.5 mM hydrogen tetrachloroaurate(III) tetrahydrate ($HAuCl_4 \cdot 4H_2O$), after which 0.6 mL of ice-cold 0.01 M $NaBH_4$ was added with vortex mixing for 2 min. The resulting seed solution became brownish yellow; it was then aged for 30 min at room temperature before use. The GNR growth solution comprised 50 mL of 1 mM $HAuCl_4 \cdot 4H_2O$ (50 mL) that was initially mixed with 50 mL of 0.2 M CTAB solution with subsequent addition of 4 mM $AgNO_3$ (1.2 mL) and 7.9 mM ascorbic acid aqueous solution (0.7 mL) with magnetic stirring, which changed the color from dark yellow to colorless. As the final step, 60 μL of the seed solution was added into the growth solution with gentle stirring, which changed the color to dark red within 1 h. The excess CTAB surfactant was removed from the final product by washing with DI water twice. The purified GNRs were PEGylated using *m*PEG-SH (MW 1,000, Laysan Bio) to enhance the stability, and the PEG-conjugated GNRs were then transferred into absolute ethanol for the next step.

Preparation of GO-IO Composites. Amine functional groups were introduced onto the surface of the Fe_3O_4@SiO_2 (IO) nanoparticles using 3-aminopropyltriethoxysilane (APTS, Sigma-Aldrich) in absolute ethanol with vigorous stirring for 6 h at room temperature. The resulting IO nanoparticles were then washed thrice with DI water. Cross-linking between the primary amine groups of IO and the carboxylic acid groups of GO was accomplished using a 1-ethyl-3-(3-dimethylaminopropyl) carbodiimide (EDC, Thermo Scientific)/*N*-hydroxysuccinimide (NHS, Thermo Scientific) coupling reaction with overnight stirring at room temperature.[1] The magnetically separated GO-IO was purified by washing with DI water *via* centrifugation and then redispersed into absolute ethanol to complete the silane-coupling reaction for hybridization of GNRs.

Preparation of GO-IO-GNR Nanocomposites. The PEGylated GNRs in the absolute ethanol were modified *via* silane functionalization using 3-mercaptopropyltrimethoxysilane (MPTS, Sigma-Aldrich) with vigorous stirring for 3 h at room temperature. The remaining excess reagents in the resulting solution were removed by centrifugation and washing thrice with absolute ethanol. The silane-capped GNRs were coupled with the GO-IO composites by vigorous stirring overnight at room temperature; the supernatant was decanted and discarded after isolating the GO-IO-GNR product by a magnet.

Results and Discussion

As well documented by D. C. Marcano *et al*., the advantage of using improved Hummers method is not produce toxic NO_x gas owing to using H_3PO_4 instead of $NaNO_3$.[16] Figure 1(a) shows a transmission electron microscopy (TEM) image of the as-prepared GO nanosheets obtained from the modified Hummers method. The exfoliated GO nanosheets are of submicrometer dimension, have a smooth surface, and wrinkled edges. A typical peak at 230 nm and a shoulder peak at 301 nm were observed in the UV-Vis spectrum of the GO suspension shown in Figure 1(b). As well documented in previous reports, the former peak can be attributed to $\pi \rightarrow \pi^*$ transitions in the π-conjugated sp^2 domains and the latter peak indicates $n \rightarrow \pi^*$ transitions in the sp^3 domain involving the carboxyl/carbonyl groups derived from the chemical exfoliation method.[19] The data suggest that the present GO nanosheets are structurally consistent with the previously reported GO.[16]

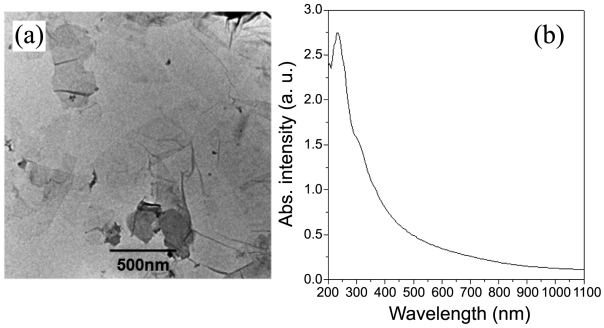

Figure 1. (a) TEM image and (b) UV-Vis absorption spectrum of graphene oxide.

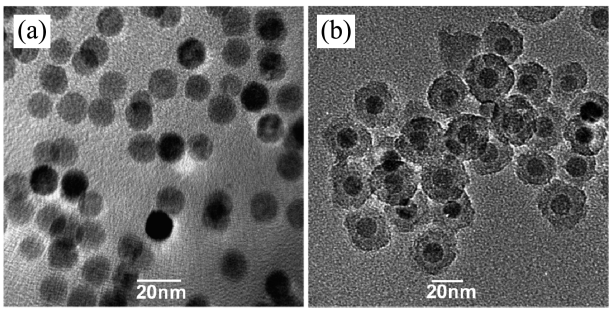

Figure 2. TEM images of (a) bare Fe_3O_4 nanoparticles and (b) Fe_3O_4@SiO_2 nanoparticles.

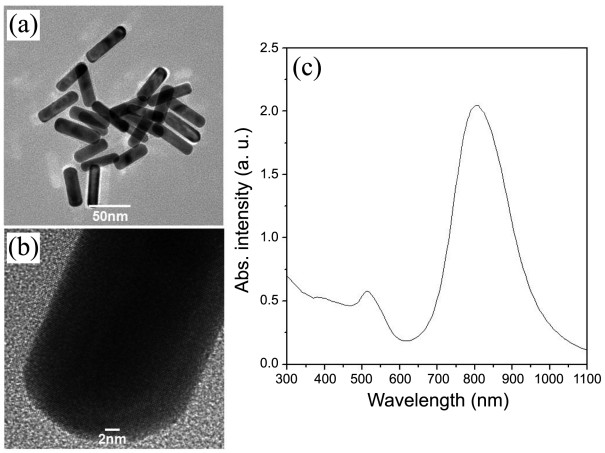

Figure 3. (a), (b) TEM and HR-TEM images, and (c) UV-Vis absorption spectrum of gold nanorods.

Figure 2 shows the TEM images of the bare Fe_3O_4 nanoparticles having a diameter of 13 ± 2.5 nm and of silica-coated Fe_3O_4@SiO_2 nanoparticles with a silica thickness of 10 ± 1.0 nm. Because of the thinness of the silica coating layer, the overall size of the resulting Fe_3O_4@SiO_2 nanoparticles is only 23 ± 3.5 nm and the nanoparticles remained well dispersed in the solvent for a few weeks without any evidence of aggregation.

Figure 3(a) shows a TEM image of the as-prepared GNRs, having an aspect ratio of approximately 3-4.

Based on recent crystallographic studies, the GNRs prepared *via* the seed-mediated growth method have rounded rectangular ends with {250} side facets because of the surface reconstruction process that minimizes the growth of the thermodynamically unfavorable {110} facets.[20] The high-resolution TEM image shown in Figure 3(b) illustrates that the present GNRs are characterized by the typical round-ended morphology. Figure 3(c) shows the UV-Vis absorption spectrum of the GNRs dispersed in DI water. The strong LSPR peak centered at approximately 804 nm corresponds to GNRs with an aspect ratio of 3-4, which is highly congruent with the TEM results.

Scheme 1 represents the procedure for synthesis of the GO-IO-GNR nanocomposites from the as-prepared GO, IO, and GNR. Already, there is an extensive amount of literature devoted to the incorporation of various nanoparticles into the GO surface *via* Van der Waals or electrostatic interactions; however, such an assembly may be easily separated owing to the weak binding forces.[21,22] Thus, we attempted to prepare the GO-IO-GNR hybrid complex through covalent bonding by using bi-functional cross-linking agents. In brief, first, the amine-functionalized Fe_3O_4@SiO_2 nanoparticles were prepared using APTS; then, the primary amine of Fe_3O_4@SiO_2 was covalently bonded to the carboxyl group of the GO surface by the EDC/NHS coupling reaction. For GNR hybridization, the silane-modified GNRs were obtained from the reaction the PEGylated GNR with MPTS and were then bonded to a silica layer of the Fe_3O_4@SiO_2 or hydroxide group of the GO surface, as summarized in Scheme 1.

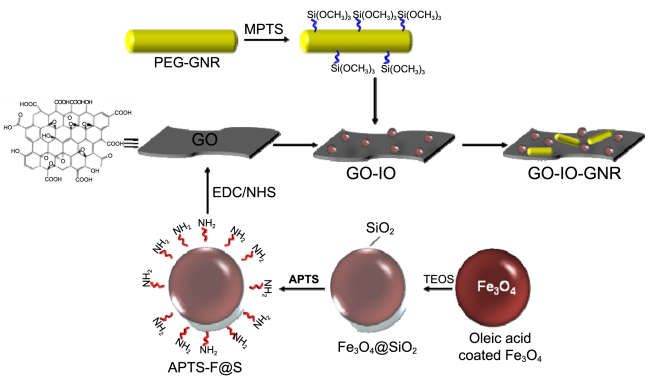

Scheme 1. Schematic representation of GO-IO-GNR nanocomposites preparation by using bi-functional cross-linking agent.

Figures 4(a) and (b) show the TEM images of the as-prepared GO-IO and GO-IO-GNR nanocomposites. Numerous Fe_3O_4@SiO_2 nanoparticles and GNRs are well anchored on the GO nanosheets. Notably, the high-magnification TEM image shows the GNRs conjugated with a silica layer of the Fe_3O_4@SiO_2 nanoparticle *via* the silane-coupling reaction, as shown in the inset of Figure 4(b).

As shown in Figure 5, the UV-Vis absorption spectrum of

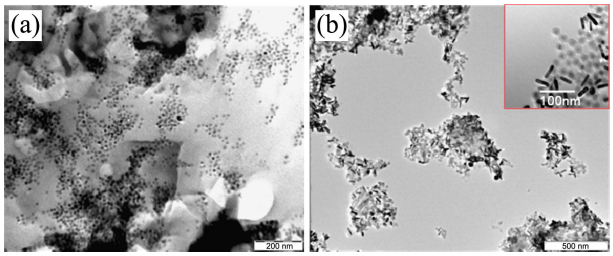

Figure 4. TEM images of (a) GO-IO and (b) GO-IO-GNR nanocomposites.

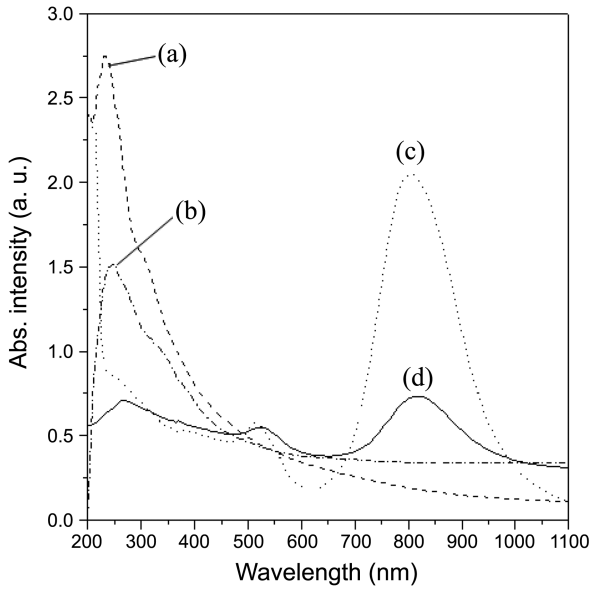

Figure 5. UV- UV-Vis absorption spectrum of (a) GO, (b) GO-IO, (c) GNR, and (d) GO-IO-GNR.

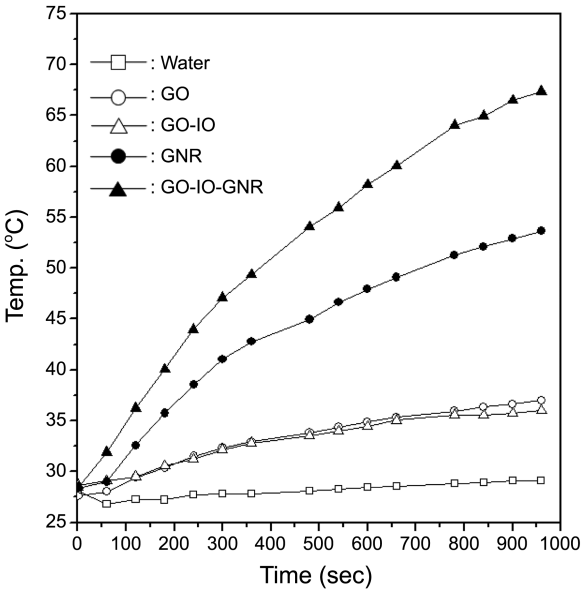

Figure 6. Temperature variation of 5 different samples upon laser (λ = 780 nm, power density = 2 mW/cm^2) irradiation time.

the GO-IO-GNR assembly displayed obvious UV-Vis absorption peaks typical of GO, IO, and GNR.

Figure 6 shows a temperature variation plot for five different samples (DI water, GO, GO-IO, GNR, and GO-IO-GNR suspensions dispersed in DI water) as a function of the NIR laser (λ = 780 nm) irradiation time. It should be mentioned that the power density (2 mW/cm^2) of the present NIR laser is 1,000 times lower than the laser power density (> 2 W/cm^2) commonly used in previous reports.[1,10,11] Before analyzing the photothermal effect, the concentration of gold in the GNR and the GO-IO-GNR samples was confirmed and adjusted based on the inductive coupled plasma (ICP) analysis. For the GO and GO-IO systems, the temperature remained almost constant at 36 °C after 16 min of laser irradiation; thus, the black color of the GO and GO-IO solution induced only a slight increase in temperature. In addition, this observation suggests an insignificant influence of the Fe_3O_4@SiO_2 nanoparticles on the photothermal effect. In contrast, the temperature of the GNR solution (97 μg Au/mL) increased to 53 °C after laser irradiation for 16 min, indicating that the LSPR of the GNR contributes to this large increase in temperature, as is well documented. For the GO-IO-GNR solution having a gold concentration similar to that of the GNR colloid, the temperature increased remarkably to 67 °C; thus, the rate of temperature increase of 4.2 °C/min is much faster than the rate of 3.3 °C/min for the GNR solution. It seems reasonable to assume that the significant enhancement of the photothermal effect observed in the GO-IO-GNR system is derived from the increased GNR density per unit area compared to the GNR colloid. Despite the preponderance of evaluations of the GNR-based photothermal effect and its biomedical applications,[1,9,12,13] there is a dearth of data on the enhanced photothermal effect of GNR, the current report being, to the best of our knowledge, the first to describe the boost in the photothermal efficiency derived from the integration of GNR into the GO nanosheets.

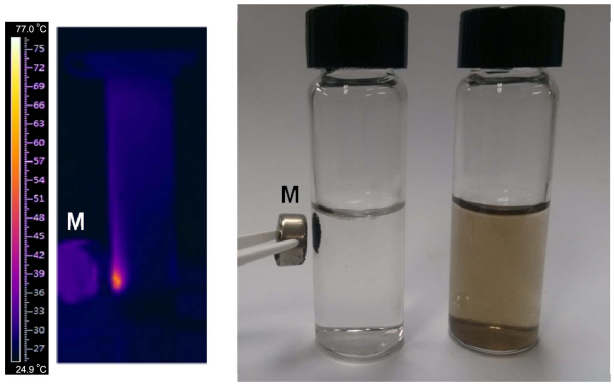

Figure 7. Photo image (right panel) of GO-IO-GNR solution and its magnetic agglomeration. IR camera image (left panel) of magnetically sorted GO-IO-GNR after laser irradiation for 3 min.

One of the most well-known applications of GO-based materials is water purification *via* adsorption and photocatalytic degradation of environmental pollutants by exploiting the large surface area (2,600 m^2/g) of the GO nanosheets and the semiconducting property of the sp^3-hybridized carbon domains.[21,22] However, the application of these species is often limited because of the difficulty associated with recycling GO; thus, GO-IO composites have instead gained prominence in eco-friendly material sciences.[23] The photo images on the right side of Figure 7 show the water-dispersed GO-IO-GNR suspension and the nanocomposites separated using a magnet. This facile separation suggests that the GO-IO-GNR composites could be easily recycled by a magnetic sorting method.

Moreover, one of the outstanding features is that local photothermal heating is possible with the GO-IO-GNR assembly *via* magnetic enrichment, as shown in the IR camera image on the left of Figure 7. It is noteworthy that the temperature of the magnetic agglomerate of the GO-IO-GNR increased rapidly to 64 °C upon laser irradiation for 3 min, whereas the respective temperatures of the GNR and the GO-IO-GNR solution remained at 36 °C and 40 °C under the same conditions. Recently, Galanzha et al. reported *in vivo* magnetic sorting and photoacoustic detection of circulating tumor cells (CTCs) by using both magnetic nanoparticles and gold-coated carbon nanotubes; metastasis-induced CTCs are known as the main cause of most cancer deaths.[24] However, their approach required a time-consuming and complicated process because of the separate use of magnetic nanoparticles for the CTC enrichment and gold-coated carbon nanotubes for photoacoustic imaging of the CTC. Therefore, they also suggested that additional challenging research should be required to further develop their study by using gold-magnetic nanoparticle complexes. Thus, we believe that the present GO-IO-GNR nancomposites may be ideal materials not only for sensitive detection but also for selective elimination of CTCs in blood vessels.

Conclusion

In summary, GO-IO-GNR nanocomposites were successfully synthesized using bifunctional cross-linking agents. The photothermal conversion efficiency of the GO-IO-GNR composite is superior to that of GNRs owing to the high density of GNRs on GO nanosheets. To the best of our knowledge, the present study provides groundbreaking empirical evidence to substantiate the enhanced photothermal effect derived from GNR-integrated nanostructures. Moreover, the Fe_3O_4@SiO_2 nanoparticles on the GO nanosheets enabled recycling of the GO-IO-GNR composites. Notably, magnetic separation of the GO-IO-GNR assembly enabled local heating *via* the photothermal method. The present results are expected to find utility in several promising applications such as theragnosis of CTCs and local heating elimination of environmental pollutants.

Acknowledgments. This paper was supported by Research Fund (project No. 2011-104-154), Kumoh National Institute of Technology. Contribution of K.-H. Yun and S.-H. Seo is same in this paper.

References

1. Cha, E.-J.; Jang, E.-S.; Sun, I.-C.; Lee, I. J.; Ko, J. H.; Kim, Y. I.; Kwon, I. C.; Kim, K.; Ahn, C.-H. *J. Controlled Release* **2011**, *155*, 152-158.
2. Jang, E.-S.; Shin, J.-H.; Ren, G.; Park, M.-J.; Cheng, K.; Chen, X.; Wu, J. C.; Sunwoo, J. B.; Chen, Z. *Biomaterials* **2012**, *33*, 5584-5592.
3. Wang, Y.; Liu, Y.; Luehmann, H.; Xia, X.; Wan, D.; Cutler, C.; Xia, Y. *Nano Lett.* **2013**, *13*, 581-585.
4. Zhou, Z.; Wang, L.; Chi, X.; Bao, J.; Yang, L.; Zhao, W.; Chen, Z.; Wang, X.; Chen, X.; Gao, J. *ACS Nano* **2013**, *7*, 3287-3296.
5. Mazzucchelli, S.; Colombo, M.; Verderio, P.; Rozek, E.; Andreata, F.; Galibiati, E.; Tortora, P.; Corsi, F.; Prosperi, D. *Angew. Chem. Int. Ed.* **2013**, *52*, 3121-3125.
6. Yong, K.-T.; Law, W.-C.; Hu, R.; Ye, L.; Liu, L.; Swihart, M. T.; Prasad, P. N. *Chem. Soc. Rev.* **2013**, *42*, 1236-1250.
7. Chen, N.; He, Y.; Su, Y.; Li, X.; Huang, Q.; Wang, H.; Zhang, X.; Tai, R.; Fan, C. *Biomaterials* **2012**, *33*, 1238-1244.
8. Huo, S.; Ma, H.; Huang, K.; Liu, J.; Wei, T.; Jin, S.; Zhang, J.; He, S.; Liang, X.-J. *Cancer Res.* **2013**, *73*, 319-330.
9. von Maltzahn, G.; Park, J.-H.; Argawal, A.; Bandaru, N. K.; Das, S. K.; Sailor, M. J.; Bhatia, S. N. *Cancer Res.* **2009**, *69*, 3892-3900.
10. Jokerst, J. V.; Thangaraj, M.; Kempen, P. J.; Sinclair, R.; Gambhir, S. S. *ACS Nano* **2012**, *6*, 5920-5930.
11. Jang, B.; Kim, Y. S.; Choi, Y. *Small* **2011**, *7*, 265-270.
12. Choi, W. I.; Kim, J.-Y.; Kang, C.; Byeon, C. C.; Kim, Y. H.; Tae, G. *ACS Nano* **2011**, *5*, 1995-2003.
13. Burke, A. R.; Singh, R. N.; Carroll, D. L.; Wood, J. C. S.; D'Agostino, R. B., Jr.; Ajayan, P. M.; Torti, F. M.; Torti, S. V. *Biomaterials* **2012**, *33*, 2961-2970.
14. Balandin, A. A.; Ghosh, S.; Bao, W. Z.; Calizo, I.; Teweldebrhan, D.; Miao, F.; Lau, C. N. *Nano Lett.* **2008**, *8*, 902-907.
15. Zhu, Y.; Murali, S.; Cai, W.; Li, X.; Suk, J. W.; Rotts, J. R.; Ruoff, R. S. *Adv. Mater.* **2010**, *22*, 3906-3924.
16. Marcano, D. C.; Kosynkin, D. V.; Berlin, J. M.; Sinitskii, A.; Sun, Z.; Slesarev, A.; Alemany, L. B.; Lu, W.; Tour, J. M. *ACS Nano* **2010**, *4*, 4806-4814.
17. Jang, E.-S. *J. Korean Chem. Soc.* **2012**, *56*, 478-483.
18. Jana, N. R.; Gearheart, L.; Murphy, C. J. *J. Phys. Chem. B* **2001**, *105*, 4065-4067.
19. Matsumoto, Y.; Koinuma, M.; Ida, S.; Hayami, S.; Taniguchi, T.; Hatakeyama, K.; Tateishi, H.; Watanabe, Y.; Amano, S. *J. Phys. Chem. C* **2011**, *115*, 19280-19286.
20. Park, K.; Drummy, L. F.; Wadams, R. C.; Koerner, H.; Nepal, D.; Fabris, L.; Vaia, R. A. *Chem. Mater.* **2013**, *25*, 555-563.
21. Liu, J.; Bai, H.; Wang, Y.; Liu, Z.; Zhang, X.; Sun, D. D. *Adv. Funct. Mater.* **2010**, *20*, 4175-4181.
22. Wang, J.; Tsuzuki, T.; Tang, B.; Hou, X.; Sun, L.; Wang, X. *Appl. Mater. Interfaces* **2012**, *4*, 3084-3090.
23. Dong, Y.; Li, J.; Shi, L.; Xu, J.; Wang, X.; Guo, Z.; Liu, W. *J. Mater. Chem. A* **2013**, *1*, 644-650
24. Galanzha, E. I.; Shashkov, E. V.; Kelly, T.; Kim, J.-W.; Yang, L.; Zharov, V. P. *Nature Nanotech.* **2009**, *4*, 855-860.